Detection of middle to late Holocene Icelandic cryptotephras in the Netherlands: tephra versus biogenic silica

M.P.E Visser, department of Earth Sciences, Faculty of Science, Utrecht University, September 2011

Abstract

Every volcano erupts ash that is characteristic for that volcano. When tephra is produced, prevailing winds can transport the tephra over large distances, where they are then deposited due to gravitational and/or precipitational fallout. The goal of this paper is to detect and chemically analyse middle to late Holocene cryptotephras in the Netherlands and trace these tephras back to their source. The Rheinberg and Zijderveld cores are sampled and a separation method based on heavy liquid separation was adapted for use on clay-rich material. Instead of ashing the samples in a furnace, which would result in producing bricks from the clay, H_2O_2 is used to dissolve all the organic material. The material is then subjected to heavy liquid separation. The particles remaining were then analysed with the optical microscope and a tephra shard count was done. The particles were deemed tephra based on their morphology and optical properties. However, after chemical analysis using the SEM, all of these supposed tephra particles turned out to be biogenic silica or mica. No Icelandic tephras were present. The biogenic silica was mistaken to be tephra due to its tephra-like morphology and the same optical properties. The absence of tephras can be explained in three possible ways: 1) the ashcloud did not extend as far as the Rheinberg and Zijderveld localities, 2) the deposition occurred by wet fallout and since there was no precipitation in the Netherlands there was no tephra deposition and 3) the localities were not suitable for deposition of tephra due to the possible presence of running water.

1. Introduction

Explosive volcanic eruptions can produce volcanic ash by two basic mechanism; 1) degassing and 2) hydrovolcanic eruptions (Heiken, 1974; Wohletz, 1983). In the first case exsollution and expansion of gasses at the surface cause the magma to loose its coherence. In the case of a hydrovolcanic eruption the magma cools very rapidly due to contact with water. Stresses in the cooled magma cause fragmentation of the magma into small glassy particles (Heiken, 1974; Wohletz, 1983). The fragmented melt particles, termed tephra, are blown high into the atmosphere. Prevailing winds can transport the ash plume over vast distances, across oceans and continents. Gravitational and precipitational fallout causes deposition of the tephra far from the source (Van den Bogaard and Schmincke, 2002). The further away from the source, the fewer and smaller the deposited ash particles. When the tephra can no longer be detected in the sediments by the naked eye and are only present in very small quantities the tephra is termed cryptotephra (Lowe and Hunt, 2001). Every volcano erupts material that is characteristic for that volcano or even that pariticular eruption. This is due to evolutionary processes that occur within the magma prior to eruption, such as magma mixing and fractional crystallization. This characteristic chemical composition is also recorded in the tephra. Therefore, distal tephras can be chemically analysed and traced back to the source eruption (Van den Bogaard and Schmincke, 2002).

Previous studies have shown that the Holocene Icelandic tephras Hekla 3, Hekla S and Hekla 4 are very wide spread in the direction southeast of Iceland. Both the Hekla 3, Hekla S and Hekla 4 tephras are found in west-central Sweden (Zillen et al., 2002; Bergman et al., 2004). The Hekla 4 tephra has also been detected in the south of Scotland (Langdon and Barber,2004), northern England (Pilcher and Hall, 1996) and Ireland (Pilcher et al., 1995; Pilcher et al., 1996).

Research on distal tephras in northern Germany revealed that several cryptotephra layers were present in Holocene peatbogs (Van den Bogaard and Schmincke, 2002). These tephras could be traced back to the following source eruptions (Van den Bogaard et al., 1994; Van den Bogaard and Schmincke, 2002):

Askja (1875 AD)
Hekla 3 (2879 ± 34 yr BP)
Hekla Selsund (3500 yr BP)
Hekla 4 (3826 ± 12 yr BP)
Hekla 5 (6036 ± 20 yr BP)

These are all eruptions of Icelandic volcanic systems.
It is expected that when looking at Holocene sediments in the Netherlands the same tephras may be found. This is expected because in countries in the proximity of the Netherlands these tephras are already found and it is possible that the ash clouds also extended over the Netherlands. The cryptotephras in Germany have already shown that tephras from Icelandic volcanic systems are more widespread than previously thought (Van den Bogaard and Schmincke, 2002).
The goal of this research is to detect and chemically analyse middle to late Holocene cryptotephras in the Netherlands and trace these tephras back to their source using geochemical fingerprinting. Thereby, this research is an addition to tephrochronology. Tephra layers are time-parallel markers between different stratigraphical records and are very reliable for correlation between stratigraphical sequences. Tephrochronology can also be used to correlate marine, terrestrial and ice-core records as well as testing age-depth models (Davies, 2005). Therefore tephrochronology can be indirectly used for example to determine whether climate change was simultaneously occurring in different localities (Lowe, 2001).

2. Methods

2.1 Selection of the cores

Two cores have been selected for analysis on the basis of them having been dated and having been taken in quiet sedimentary settings.
The first core that has been selected is the Rheinberg core. This core has been taken in a paleomeander of the Rhine (fig. 1) (Erkens et al., 2011). The lithology consists of (humic) clay. Previous research produced an age-depth model for this core based on calibrated radiocarbon dates and LOI (loss-on-ignition) measurements (Minderhoud et al. 2008). The ages of the eruptions had to be converted to calibrated ages using Oxcal (table 1). This had to be done in order to compare the ages of the tephra with the ages of the eruptions. From the age-depth model resulting from the previous study it can be inferred that the Hekla S tephra was expected to be present at a depth of 335 cm. Hekla 4 was expected at a depth of 560 cm. The ages of Hekla 3 and Hekla 5 did not fall within the age range of this core.
The second core that has been selected is the Zijderveld core, which has been taken in a flood plain of the Lek (fig. 2) (Gouw and Erkens, 2007). Flood plain deposits consist of (humic) clay deposited during flooding of the plain, alternated with peat layers (fig. 3) (Gouw and Erkens, 2007). The Zijderveld core has a depth range of 90-340 cm and the lithology ranges from clay-rich peat to peaty clay and silty clay. In previous research the core has been dated using C-14 on three depth intervals (Berendsen and Stouthamer, 2001). A linear correlation between depth and calibrated age has been used to determine which depth intervals correlate with the age of the tephras expected to be present. From this model it was inferred that the Hekla 3 tephra is expected to be present at a depth of around 88 cm. In the range 90-95 cm a large piece of wood is present. Since the tephra is expected to be present in a depth range centered around 88 cm depth, it may also be present at a larger depth. Therefore, the depth interval 095-110 cm has been analysed for the presence of Hekla 3 tephra. The Hekla S tephra is expected to be present at a depth of 193 cm. The Hekla 4 tephra is expected to be present around a depth of 273 cm.

2.2 Tephra separation

The two cores Rheinberg and Zijderveld have a different lithology, which affected the method that needed to be used in order to separate the tephra from the sediment. The method that is generally used is developed for peat-rich samples and is based on ashing of the samples in a furnace in order to remove the organic matter (Van den Bogaard and Schmincke, 2002, Davies et al., 2005, Wastegard et al., 2008). However, using this method on the more clay-rich material of the Rheinberg core would result in producing bricks. Therefore a new separation method had to be developed including an alternative for removing organic material.

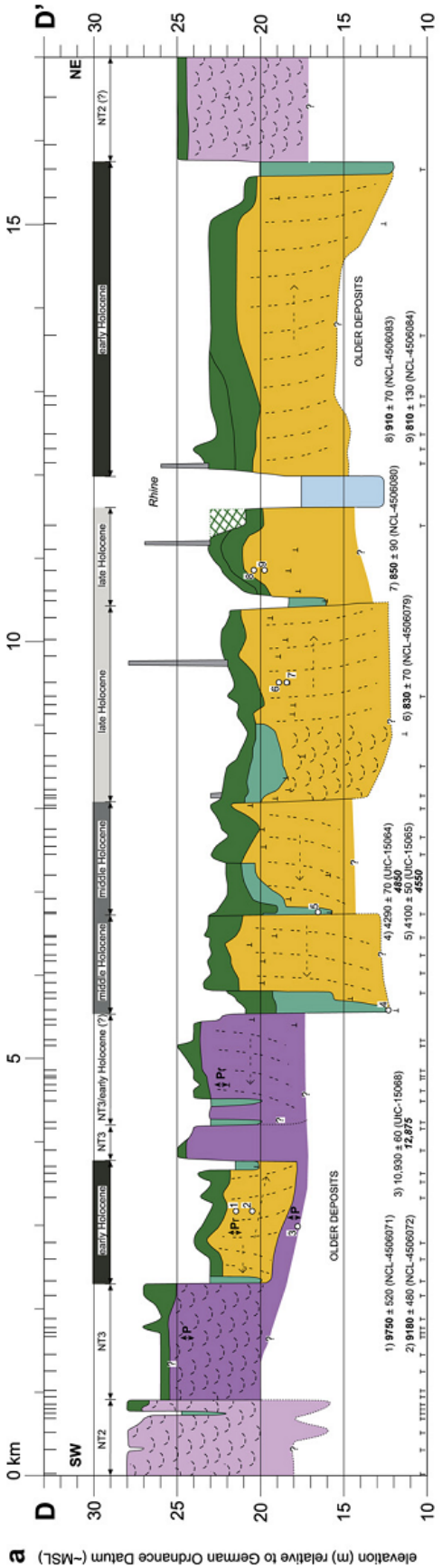

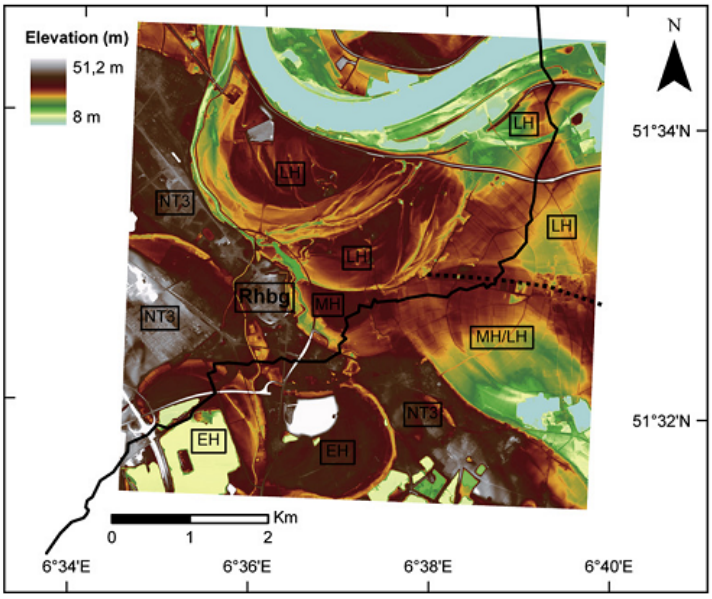

Fig 1: a) Cross section through the Rhine and the location of the Rheinberg core (at approximately 4,5 km), b) Digital elevation model of the surroundings of Rheinberg (Rhbg). (Erkens et al., 2011).

LEGEND

- channel-belt deposits (sand and gravel)
- channel-fill deposits (clay)
- natural levee deposits (sandy and silty clay)
- crevasse deposits (sand, sandy and silty clay, clay)
- floodbasin deposits (clay)
- organics (peat)
- substrate
- escarpment
- section X-X'

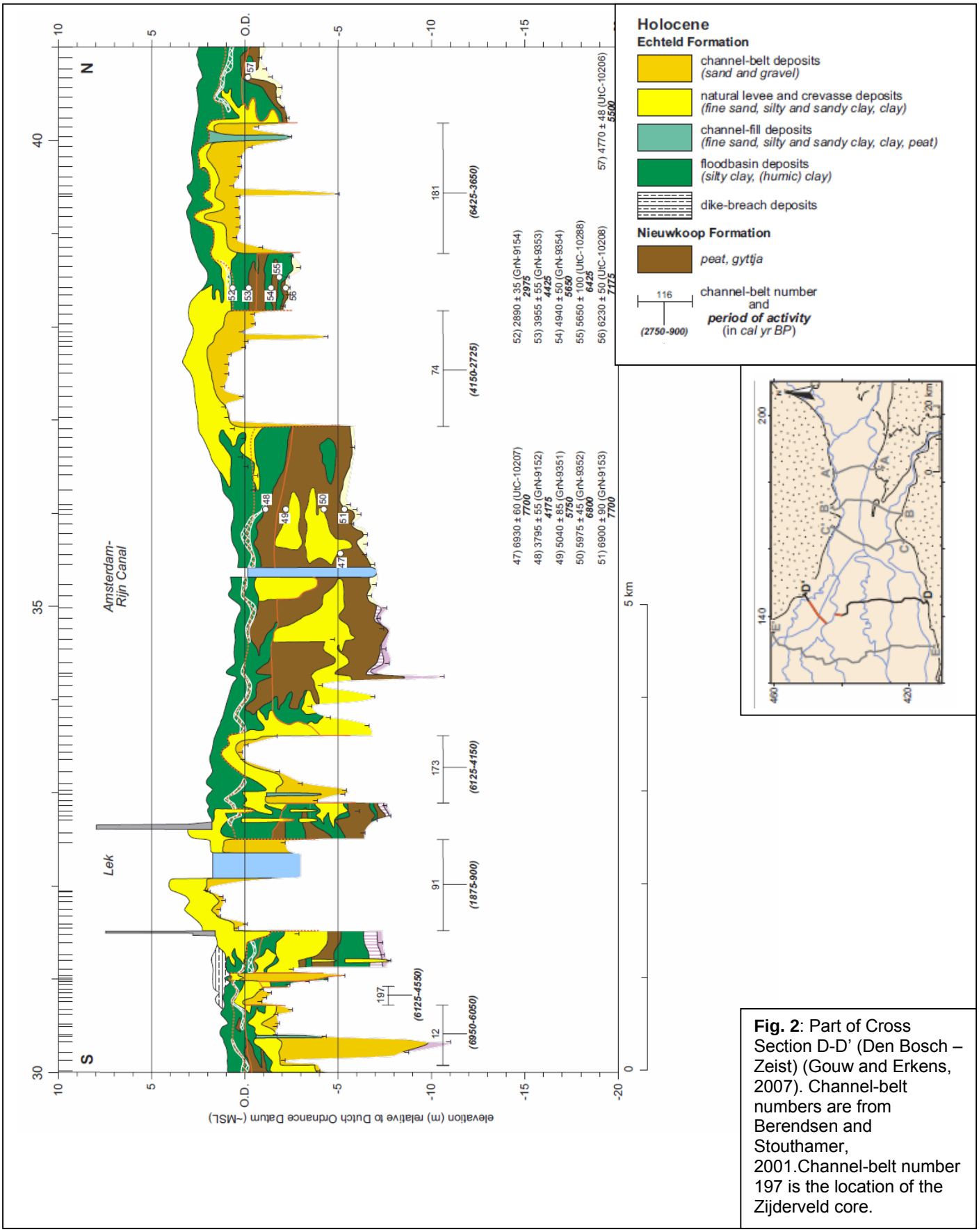

Fig. 2: Part of Cross Section D-D' (Den Bosch – Zeist) (Gouw and Erkens, 2007). Channel-belt numbers are from Berendsen and Stouthamer, 2001.Channel-belt number 197 is the location of the Zijderveld core.

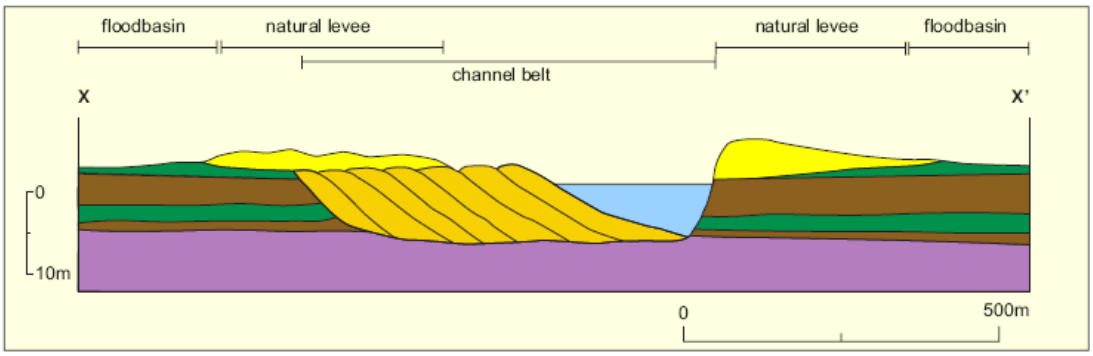

Fig. 3: Cross section of a meandering River in the Rhine-Meuse delta, showing the depositional environments. Legend see figure 2. (Gouw and Erkens, 2007).

Table 1: Tephra ages. (* Van den Bogaard and Schmincke, 2002)

Tephra	Age*	Calibrated age (Oxcal)
Hekla 3	2879 ± 34 yr BP	3014 ± 50 cal yr BP
Hekla S	3500 yr BP	3720 cal yr BP
Hekla 4	3826 ± 12 yr BP	4211 ± 31 cal yr BP
Hekla 5	6036 ± 20 yr BP	6892 ± 34 cal yr BP

Table 2: Sample intervals.

Tephra	Target depth Rheinberg (cm)	Depth interval Rheinberg (cm)	Target depth Zijderveld (cm)	Depth interval Zijderveld (cm)
Hekla 3	-	-	88	095-110
Hekla S	335	310-370	193	180-205
Hekla 4	560	510-580	273	265-285

Table 3 Comparison of tephra-like particles from sample RB340-345 and NRB340-350 with known Hekla tephras. [1] from van den Bogaard and Schminke, 2002. [2] Pilcher et al., 1996 via tephrabase.org. [3] Boygle, 1994 via tephrabase.org.

Sample	SiO_2	TiO_2	Al_2O_3	Fe_2O_3	MnO	MgO	CaO	Na_2O	K_2O	P_2O_5
RB340J	76.86	0.70	11.01	4.46	1.20	1.00	0.00	0.79	0.78	3.20
RB340K	61.31	1.16	20.49	6.24	1.80	3.55	1.23	1.95	1.83	0.44
NRB340E	79.90	0.00	12.67	1.28	0.57	1.01	0.25	0.91	2.60	0.81
NRB340G	79.27	0.94	10.07	1.67	1.05	2.46	0.54	1.19	1.78	1.03
NRB340H	60.42	0.65	20.61	1.79	0.40	1.01	0.61	12.64	0.43	1.45
NRB340J	69.53	0.00	20.07	2.45	0.00	2.15	0.64	1.68	2.38	1.10
Known tephra	**SiO_2**	**TiO_2**	**Al_2O_3**	**Fe_2O_3**	**MnO**	**MgO**	**CaO**	**Na_2O**	**K_2O**	**P_2O_5**
Hekla 4[1]	76.44	0.00	12.89	1.98	0.20	0.02	1.30	4.15	3.01	0.00
Hekla 4[1]	76.34	0.07	13.11	1.91	0.17	0.05	1.45	4.19	2.71	0.00
Hekla 4[2]	74.48	0.14	12.30	1.67	-	0.06	1.17	4.08	2.74	-
Hekla S[1]	69.64	0.14	14.91	5.01	0.25	0.09	3.38	4.45	2.05	0.07
Hekla 3[1]	69.44	0.37	15.37	4.86	0.14	0.25	2.90	4.33	2.26	0.07
Hekla 3[3]	62.84	0.74	14.89	7.64	0.21	0.86	4.28	4.02	1.76	-
Hekla 3[3]	60.83	0.74	16.86	7.16	0.24	0.78	5.22	5.13	1.37	-

Step 1	5 cm interval sampling of core	
Step 2	Add 5% HCL at 70˚C to remove carbonates	
Step 3	Add 35% H_2O_2 at 120˚C to remove organic matter.	In the case of a large amount of organic matter: 3b: Sieve through 500 µm mesh 3c: Ad H_2O_2
Step 4	Add distilled water and let suspension sink. Decant suspension containing small and light organic material. Repeat until all light material is removed.	
Step 5	Sieve with 8µm sieve. The >8µm residue is transferred to a tube.	
Step 6	Add 35% H_2O_2. Put tubes in the stove at 70˚C until all the H_2O_2 has reacted.	
Step 7	Sieve with 8µm sieve. Transfer the residue to tube.	
Step 8	Top tubes up with distilled water and centrifuge at 2500 rpm for 10 min., no brake.	
Step 9	Decant water. Add 24 ml sodium polytungstate with $\rho = 2.5\ ^{g}/_{cm^3}$. Centrifuge at 2500 rpm for 20 min., no brake.	
Step 10	Decant float into tubes marked with T (target). The float contains the tephra.	
Step 11	Top up both the T-tubes and the residue tubes with distilled water. Centrifuge at 2500 rpm for 10 min., no brake. Decant sodium polytungstate to recover.	
Step 12	Repeat previous step two times for the T-tubes.	

Fig. 4: Procedure for extraction of tephra from clay-rich samples (revised from Blockley et al., 2005).

The method developed by Blockley et al. (2005) uses heavy liquid separation to separate the tephra from mineral material and other unwanted materials like biogenic silica. Blockleys method starts with adding 10% HCL to remove the carbonates and sieving with 80 µm and 25 µm sieves to remove too small and too large material. The main part of the separation method consists of the heavy liquid separation using Sodium Polytungstate (SPT) of a density slightly higher than the density of the tephra. This will separate the tephra from the heavier mineral material present in the sample. The method of Blockley is suitable for peat-rich samples and had to be addapted to be applicable to clay-rich samples. The addapted method will be described below.

The depth ranges in which tephras were expected to be present were sampled at 5 cm intervals in order to determine whether the tephra is actually present. The sampled intervals are shown in table 2, together with the depth at which the tephra was expected. The adapted procedure for extracting tephra from clay-rich sediments is shown in figure 4. The first step after sampling was to add 5% HCl in order to remove carbonates from the sample. Instead of the usual ashing of the sample to remove the organic matter, 35% H_2O_2 was added in order to dissolve the organic material (step 3) (Koren et al., 2008). The H_2O_2 also disaggregated the sediment. The material was then subjected to a series of setteling and decanting, which is an effective way of removing the light plant material. The material was then sieved through an 8 µm mesh in order to remove all the clay minerals. The sediment has now been fully disaggregated and H_2O_2 was again added to remove the last remaining organics, followed by another step of sieving (step 7). It is important that all organic material is removed before starting the heavy liquid separation because mineral materials may be trapped in organic matter and therefore not be separated from the heavier material.
In the case of the material from the Zijderveld core, which contained more organic matter than the Rheinberg core material, two intermediate steps were added to the procedure. After adding the H_2O_2 in step 3, the sample was sieved with an 500 µm mesh in order to remove all the large organics that would have taken very long to dissolve in H_2O_2 (step 3b). Following this intermediate sieving was another step of adding H_2O_2 at 120 ˚C to further remove remaining organic matter (step 3c).
After step 7 all carbonates, organic matter and clay has been removed from the sample. Heavy liquid separation was then applied in order to separate the tephra from the heavier materials. The tephras have a density of 2.45 $^{g}/_{cm^3}$. Sodium Polyungstate (SPT) with a density of 2.5 $^{g}/_{cm^3}$ is used to separate the heavy mineral material from the tephra (Blockley et al., 2005). The cryptotephra particles are concentrated together with diatoms, sponge spicula and mineral matter with a density smaller than 2.5 $^{g}/_{cm^3}$.
SPT with densities of 2.0, 2.2 and 2.3 $^{g}/_{cm^3}$ was used in order to try and further separate the tephra from the spicula and diatoms (Blockley et al., 2005), to no effect. The diatoms and sponge spicula apparently have a density very close to that of the tephra and therefore they could not be separated from the tephra using heavy liquid separation. This is opposed to what Blockley et al. (2005) stated, namely that sponge spicula could be separates using 2.0 $^{g}/_{cm^3}$ and diatoms could be separated with SPT of a density up to 2.25 $g/_{cm^3}$.

The resulting residue containing the tephra, sponge spicula and diatoms was then mounted on slides using glycerine. The slides were analysed with the optical microscope (magnification 500x) for the presence of tephra and the amount of shards per sample were counted.
When it was determined in which depth range the tephra peak was present, the core could be resampled. Since the aim of this research is to determine if cryptotephra is present and trace the found tephra back to its source, the core has been resampled at 5 cm intervals. The samples have been taken volumetrically at 5 cm^3 in order to count the number of tephra particles per volume. The exact depth of the tephra peak is not of

importance. The tephra was again separated from the sediment using the method outlined in figure 4. For the chemical analysis the tephra had to be further separated from the diatoms, sponge spicula and mineral matter. The particles were picked manually using a single-hair brush and were deposited on a carbon stub, which is used for surface analysis with the SEM. The picking was done twice, once underneath the binocular (magnification 50x) and once underneath the optical microscope (magnification 500x). The samples picked underneath the binocular have been given the preposition N.

2.3 Chemical analysis method

The particles have been analysed using the Scanning Electron Microscope (SEM). First, the SEM was used to look at the morphology of the particles. The SEM has then been used to make a chemical analysis of the surface of the particles. This has been done in order to give a preliminary idea of whether the shards actually were tephra, what the chemical composition of the tephra was and whether the overall chemistry fitted with Hekla tephras. When it has been determined that the particles actually were tephras, they have been subjected to a more precise chemical analysis of the internal shards, using the Electron Microprobe (EMP). This more precise chemical analysis is needed in order to determine during which eruption the tephra was formed.

3. Results

3.1 Shard counts

Observations on the slides using an optical microscope revealed that cryptotephra shards were present in both cores at several intervals. The shards present in each depth interval have been counted and presented in figure 5a-e. The Rheinberg core depth interval 310-370 cm contained two very clear shard peaks. One of these peaks is expected to be Hekla S, the other peak a yet unknown tephra. The Rheinberg depth interval 510-580 cm also exhibited a shard peak, which is expected to be Hekla 4. The Zijderveld core depth interval 95-110 cm did not show a clearly defined peak, though it appeared clear that shards were present in this depth interval in a significant amount (up to 162 shards). These shards are expected to be Hekla 3. The Zijderveld core depth interval 180-205 cm exhibited a shard peak of 738 shards, which is expected to be Hekla S. The Zijderveld core depth interval 265-285 cm exhibited a peak of 579 shards between 280 and 285 cm depth.
The intervals that contained the shard peaks have been subjected to chemical analysis using the SEM.

3.2 Chemical analysis using the SEM

The samples analysed with the SEM are Rheinberg 340-345 cm, Rheinberg 345-350 cm, Rheinberg 360-365 cm, Rheinberg 547-552 cm and Zijderveld 095-100, Zijderveld195-200, Zijderveld 280-285. Chemical analysis of the particles showed them to be mica, biogenic silica (fig. 6) and unidentified material (Appendix A). The biogenic silica content of the samples ranges from approximately 50% to 90%. The biogenic silica particles in several cases have a very tephra-like morphology (fig. 7a). The EDX spectrum in figure 7b shows the composition of the biogenic silica to be almost pure SiO_2. Only the samples RB 340-345 and NRB 340-350 contained a few particles of possible tephra composition. Table 3 shows the chemistry of the possible tephras found in RB 340-345 and NRB 340-350, compared with known Hekla compositions with similar SiO_2 wt%. It can be seen that for the composition of the known Hekla tephras, the wt% of Al_2O_3, MnO, MgO and Na_2O varies only slightly with varying SiO_2 wt%. Therefore, when comparing these Hekla tephras with the samples, these elements are used. These particles are also plotted in a SiO_2 versus Al_2O_3 graph (fig. 8). It can be seen that the tephra-like particles are not Hekla tephras; for several particles the Al_2O_3 wt% is too high, for all the particles the Na_2O wt% is too low and in one case too high. The tephra-like particles with a wt% of Al_2O_3 of 19 or higher do not fit with any known Icelandic or North European tephra (Haflidason et al., 2000; tephrabase.org).

A: Rheinberg

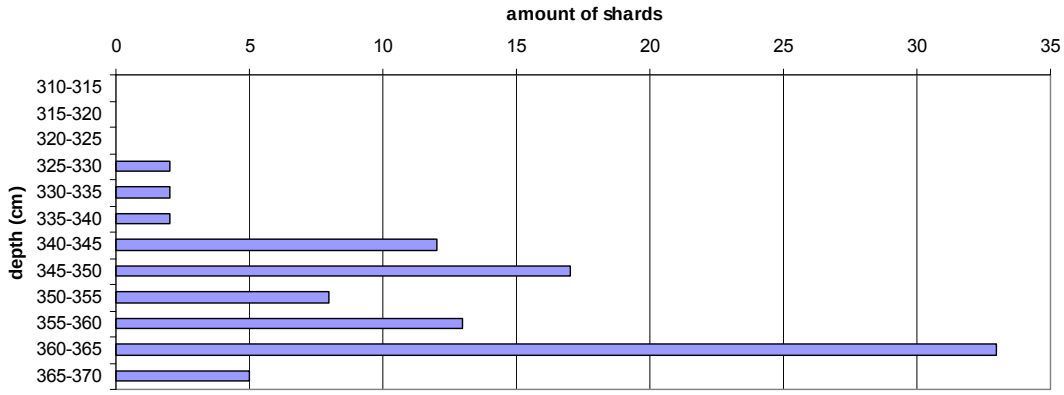

B: Rheinberg

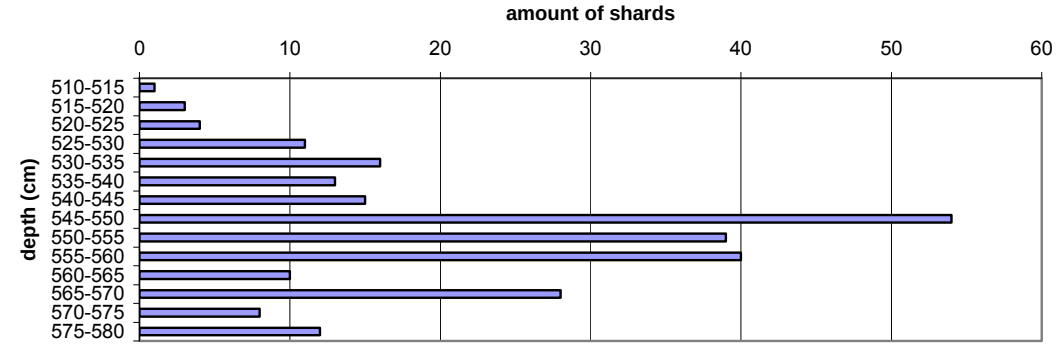

C: Zijderveld

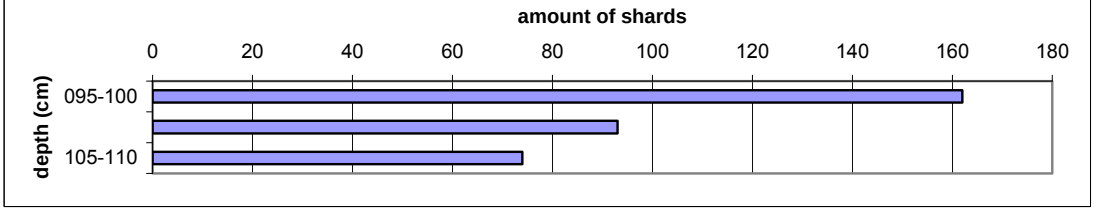

D: Zijderveld

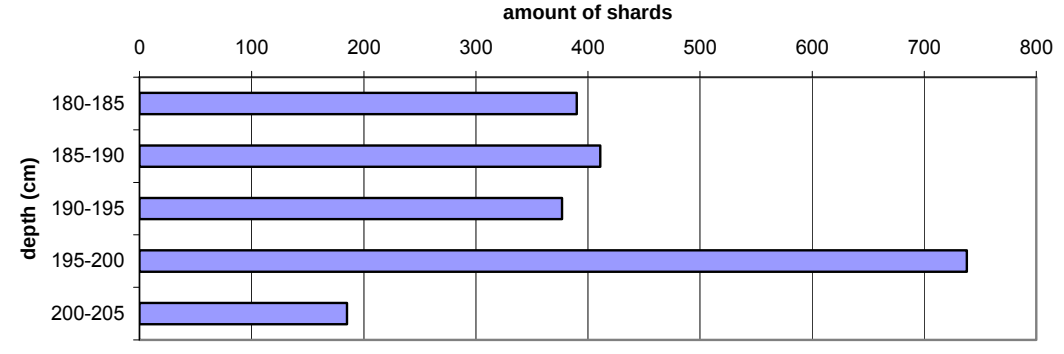

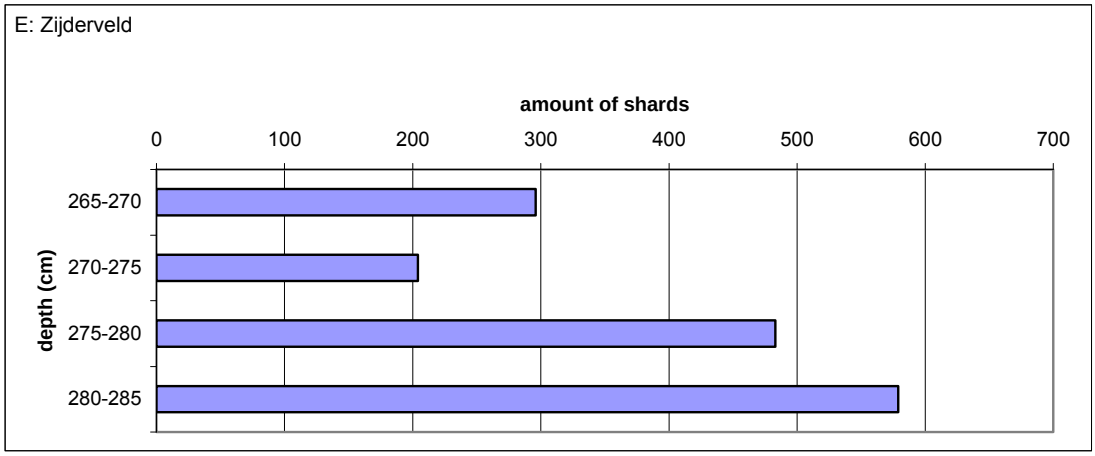

Fig. 5: Shard counts for the analysed depth intervals for the Rheinberg (a,b) and Zijderveld (c-e) cores.

The biogenic silica and micas are also plotted against known Hekla tephras (fig. 9). It can be seen that the Hekla tephras, biogenic silica and micas plot in distinct groups. The micas have a SiO_2 wt% between 40 and 50 and the Al_2O_3 wt% ranges between 15 and 40 (fig. 9a). The biogenic silicas however, have a very constant Al_2O_3 wt% between 0 and 10. The tephras also have a constant Al_2O_3 wt% between 12 and 17. When plotting SiO_2 versus alkalines (fig. 9b) it can be seen that the wt% of alkalines is constant for the Hekla tephras, while the biogenic silica and micas show a range of alkaline wt%, the micas having a higher wt% Na_2O + K_2O than the biogenic silicas. A plot of SiO_2/Al_2O_3 versus K_2O/Na_2O shows most clearly the chemical differences between the Hekla tephra, biogenic silica and mica (fig. 9c). The biogenic silica has a SiO_2/Al_2O_3 which ranges between 8 and 76, while the K_2O/Na_2O is very constant, having a value between 0 and 2. The micas however, have a constant SiO_2/Al_2O_3 of approximately 2, while the K_2O/Na_2O ranges between 0,5 and 8,5. The Hekla tephras have both a constant SiO_2/Al_2O_3 (3,6-6) and a constant K_2O/Na_2O (0,3-0,7).

3.3 Particle shape: tephra versus biogenic silica

Volcanic particle shapes are morphologically complex and variable. The shape of volcanic particles, which formed due to fragmentation processes, is controlled by exsolution of volatiles (magmatic) and/or interaction with ground- or surface water (hydrovolcanic) (Wohletz, 1983; Heiken, 1974). Magmatic fragmentation typically produces vesicular particles with cuspate shapes. The shape of these particles is controlled by factors that control the growth of vesicles in the magma, such as viscosity, temperature and volatile content of the magma. In contrast, hydromagmatic fragmentation produces fine grained (<100µm) particles, with a range of shape-types (fig. 10a – 10d) (Wohletz, 1983). The shape-types reflect the many possible variables that may influence water-magma interaction. Type 1 shape particles are blocky and equant (fig. 10). Type 1 particles are formed by low energetic forms of water-magma interaction, such as cooling-contraction granulation. The blocky particles occur together with angular and elongated splinters formed by quenching and shattering. Pyramidal shapes are also typical for type 1 shapes. The type 2, 3, 4 and 5 shapes are a product of more explosive water-magma interaction. The shapes of type 2 particles are controlled by vesicle walls. The vesicle walls are rounded and the overall shape is irregular. Type 3 shapes are moss-like and convoluted, type 4 shapes are spherical and drop-like with smooth and curved surfaces. The type 5 shapes are plate-like and characteristic of the fine fraction of vesicular magmas.

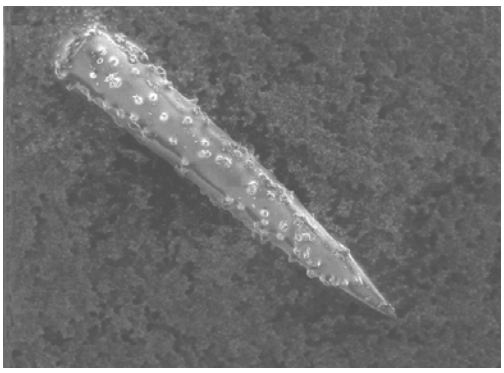

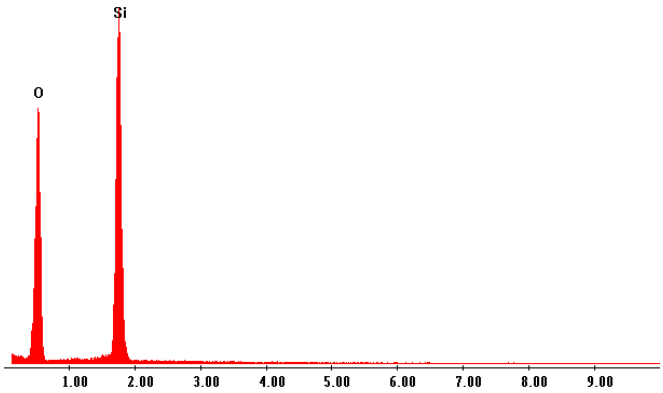

Sponge Spicula (Biogenic Silica)

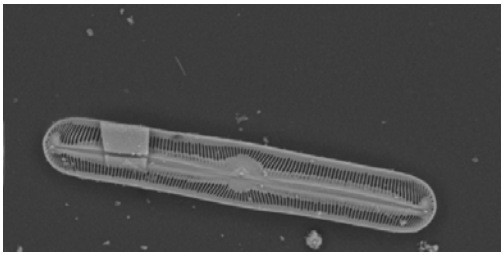

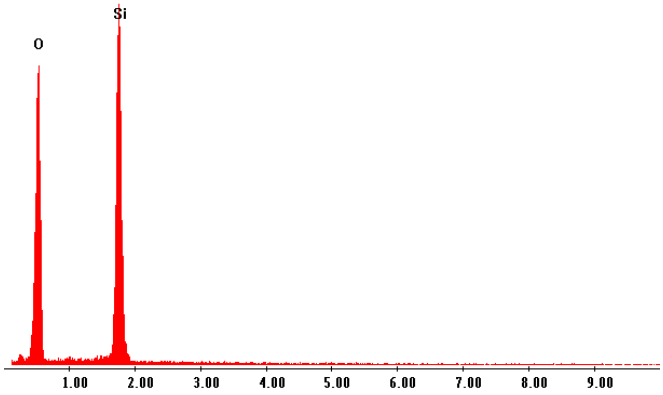

Diatom (Biogenic Silica)

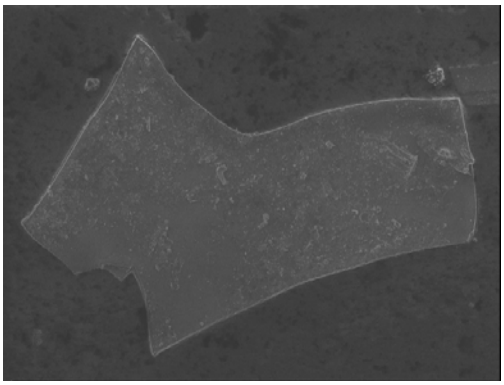

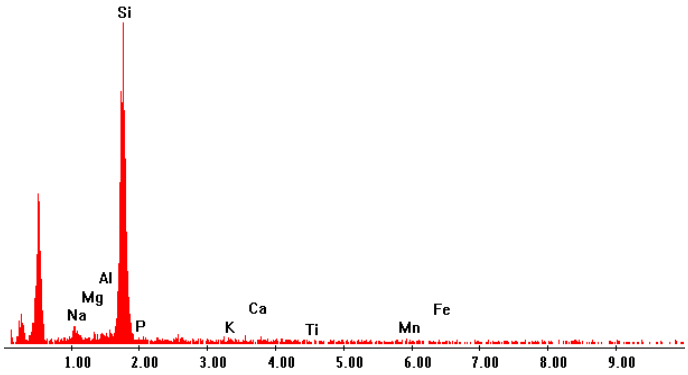

Phytolith (Biogenic Silica)

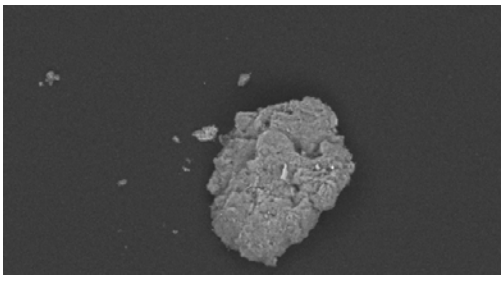

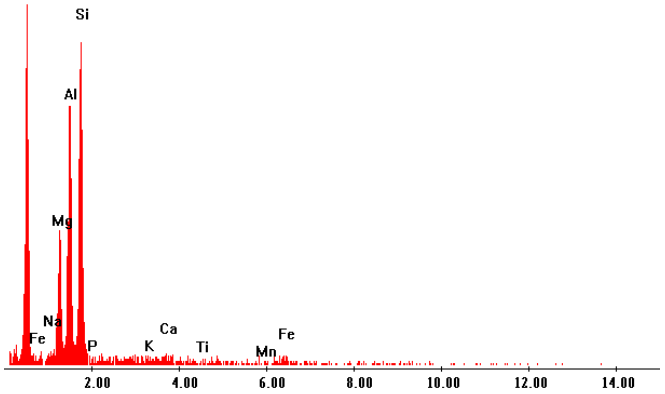

Mica

Fig. 6: Different types of particles found with chemical analysis with SEM and their EDX spectra.

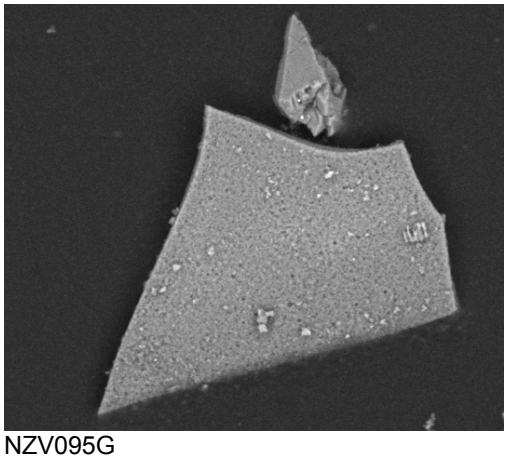

NZV095G

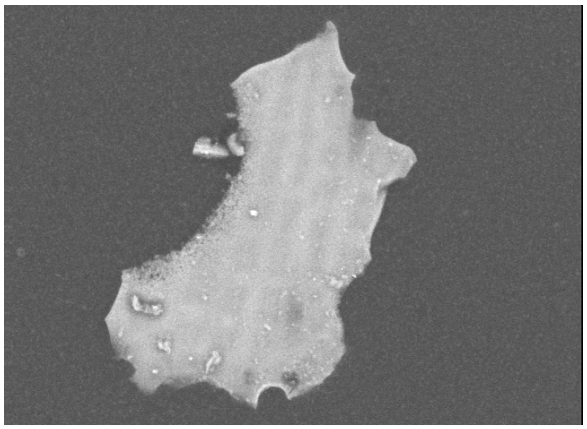

ZV195B

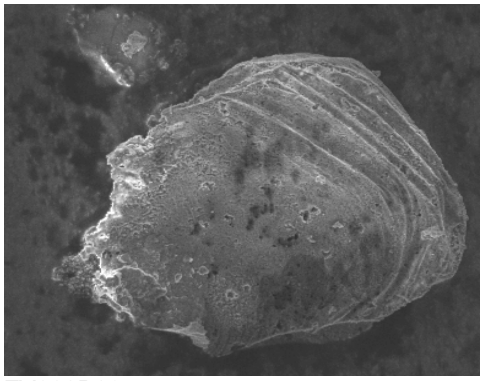

ZV280B09

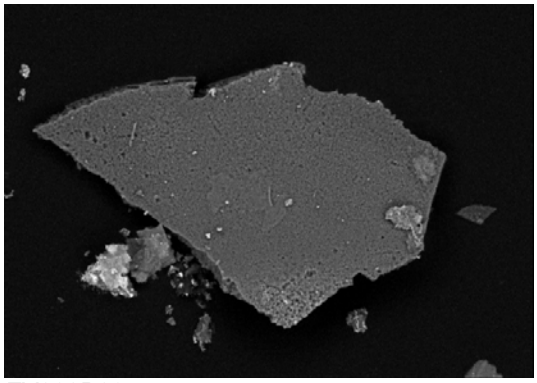

ZV280B23

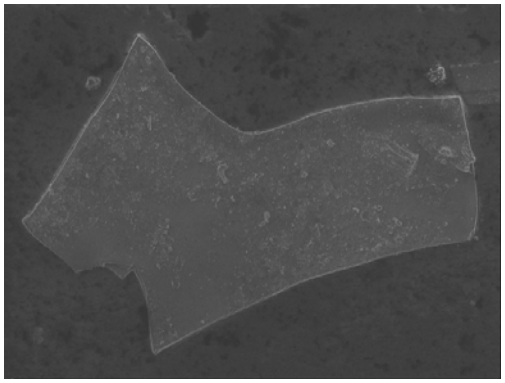

ZV280B13

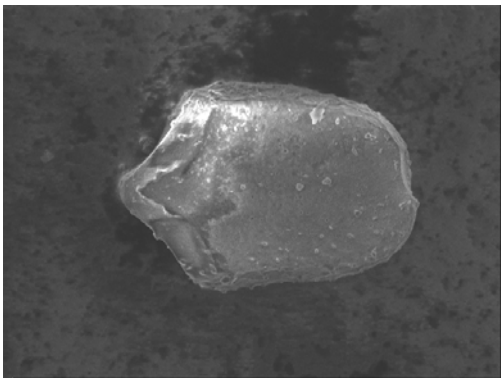

ZV280B16

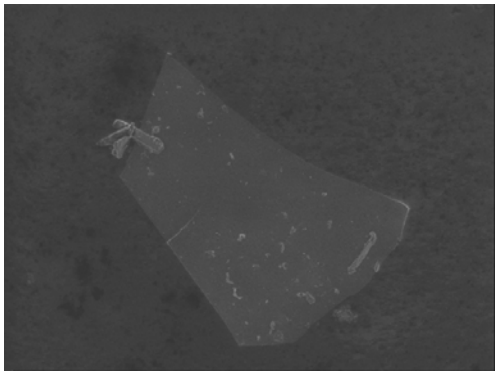

ZV280B12

Fig. 7a: Biogenic silica particles with a tephra-like morphology.

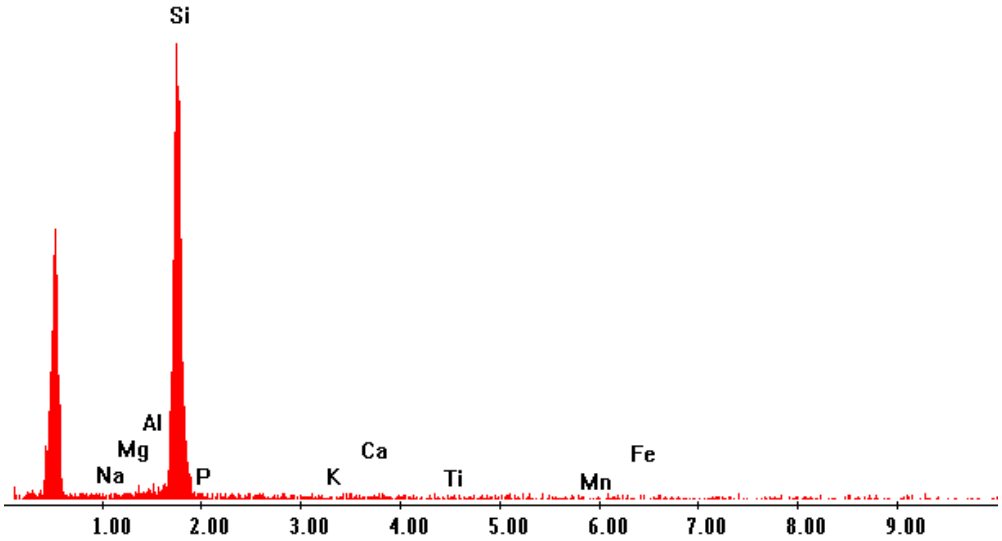

Fig. 7b: EDX spectrum representative for all biogenic silica particles represented in fig. 7a.

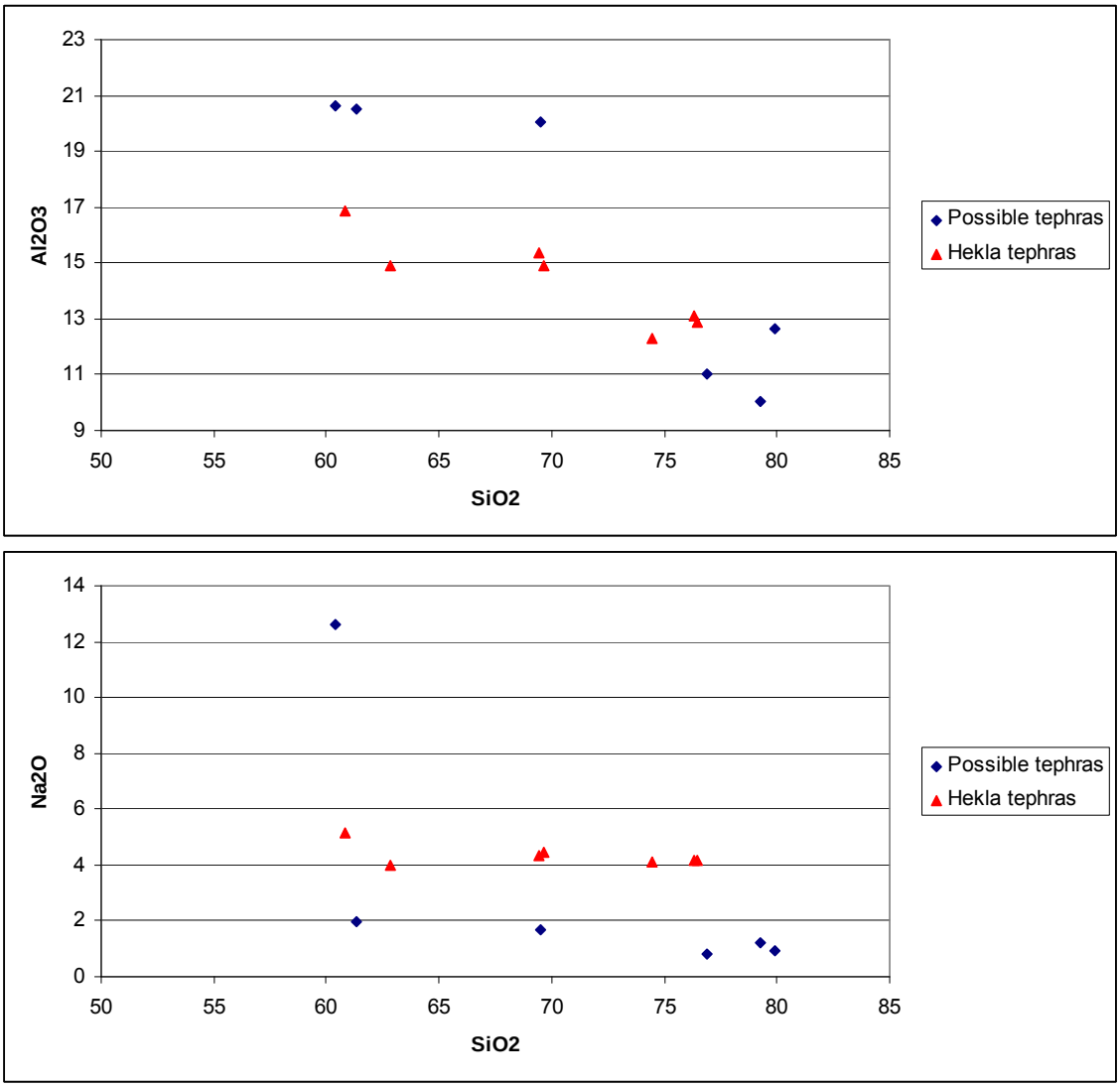

Fig. 8: Particles with possible tephra composition plotted against known Hekla tephras. The composition of the particles is shown in table 3.

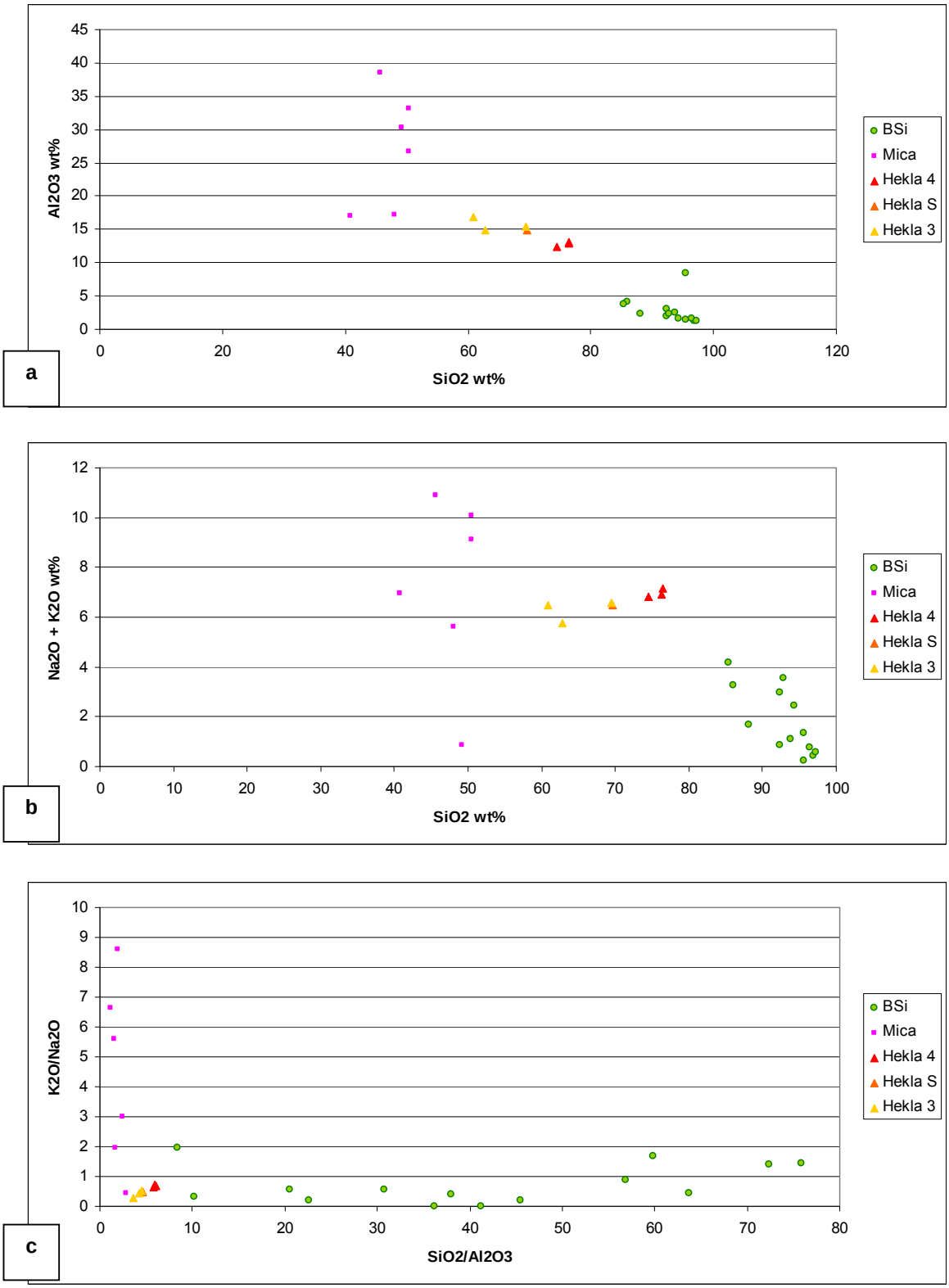

Fig. 9: Chemistry of biogenic silica (BSi) and mica plotted with known Hekla tephras.

Types 1 and 2 dominate pyroclasts greater than 100 µm in diameter. Types 3, 4 and 5 are typical of fine ash (Wohletz, 1983). In case of distal tephras it can be expected that shape-types 1 and 2 are not present. These particles will be too large and therefore too heavy to be transported through the air over large distances. Particle morphology can also be affected by later alteration caused by transportation, deposition and reworking (Maria and Carey, 2002). Figure 11 shows a range of shapes for Icelandic tephras. They also exhibit most of the shape-types as mentioned by Wohletz (1983). Obviously, there is a large variability in shard morphology.

Biogenic silica (BSi), also called biogenic opal, is a biogenic mineral formed by processes of polymerization of SiO_2. The BSi consists of pherical silica bodies which accumulate as a mass (Postek, 1981). Biogenic silica is amorphous (fig. 12). It has a glassy morphology, a high relief in plain-polarized light and is isotropic in cross-polarized light. It therefore has the same optical properties as tephra. Colours vary from colourless to light green and brownish, though the colourless variants are dominant. Biogenic silica formed in plants is called Phytolith (fig. 6). BSi can also be found in the form of diatoms (a major algae group) and sponge spicula (fig. 6). When looking at the BSi with ultra high magnification it can be seen that they have a distinctive structure (fig. 13). The sponge spiculum (fig. 13.a-e) exhibits regular protrusions on the side. The phytholith has a porous structure (fig. 13.f, 13.g), just as the diatoms (fig. 13.h), while the sponge spiculum shows a more 'pockmarked' structure (fig. 13.a-e). When the structure is compared to the mica, which is crystalline instead of amorphous, it can be seen that the structure of the mica is more smooth (fig. 13.i, 13,j).

Since the biogenic silica is amorphous it can accomodate a large range of different morphologies (Coradin and Lopez, 2003).The biogenic silica particles found in several samples have a very tephra-like morphology. A few examples of the similarity in morphology between tephra and biogenic silica are shown in figure 14.

4. Discussion

The absence of Icelandic tephra in the Rheinberg and Zijderveld cores can be explained in several ways. The first possibility is that the ash cloud just didn't extend to cover the sites of the Rheinberg core (Germany) and the Zijderveld core (the Netherlands). In that case the tephra found in Northern Germany (van den Bogaard and Schmincke, 2002) would indicate the maximum areal extent of the ash cloud. This would mean that there is no Hekla 3, Hekla S and Helka 4 tephra present in the subsurface of the Netherlands. It is also possible that the ashcloud did pass over the Netherlands and Germany, but that deposition only occurred in northern Germany. Dugmore et al. (1995) suggests that when deposition mainly occurs by wet fallout, a patchy fallout pattern would result. This would mean that the Netherlands received little or no precipitation when the ashcloud passed over, with no deposition of tephra as a result, while precipitation and therefore deposition did occur in northern Germany. A third possible explanation is that the locations of the cores, a residual channel and a flood basin, are not suitable for deposition of tephra due to the possible presence of running water.

A fourth possibility is that the age model for the cores is wrong. However, the C-14 dates taken in the cores were in several cases very close to the ages of the tephras that were expected to be present. Therefore it seems reasonable to say that the age model is adequate for determining the depth of the tephras in the cores.

The last possible explanation is that the separation method is wrong. It is possible that during the decanting of the light plant material the tephras have also been decanted. However, the sponge spicula and diatoms have a density close to that of the tephra and these are still present in the samples after decanting. Therefore it can safely be assumed that the tephras were also still in the sample after decanting, if they were present in the sample in the first place.

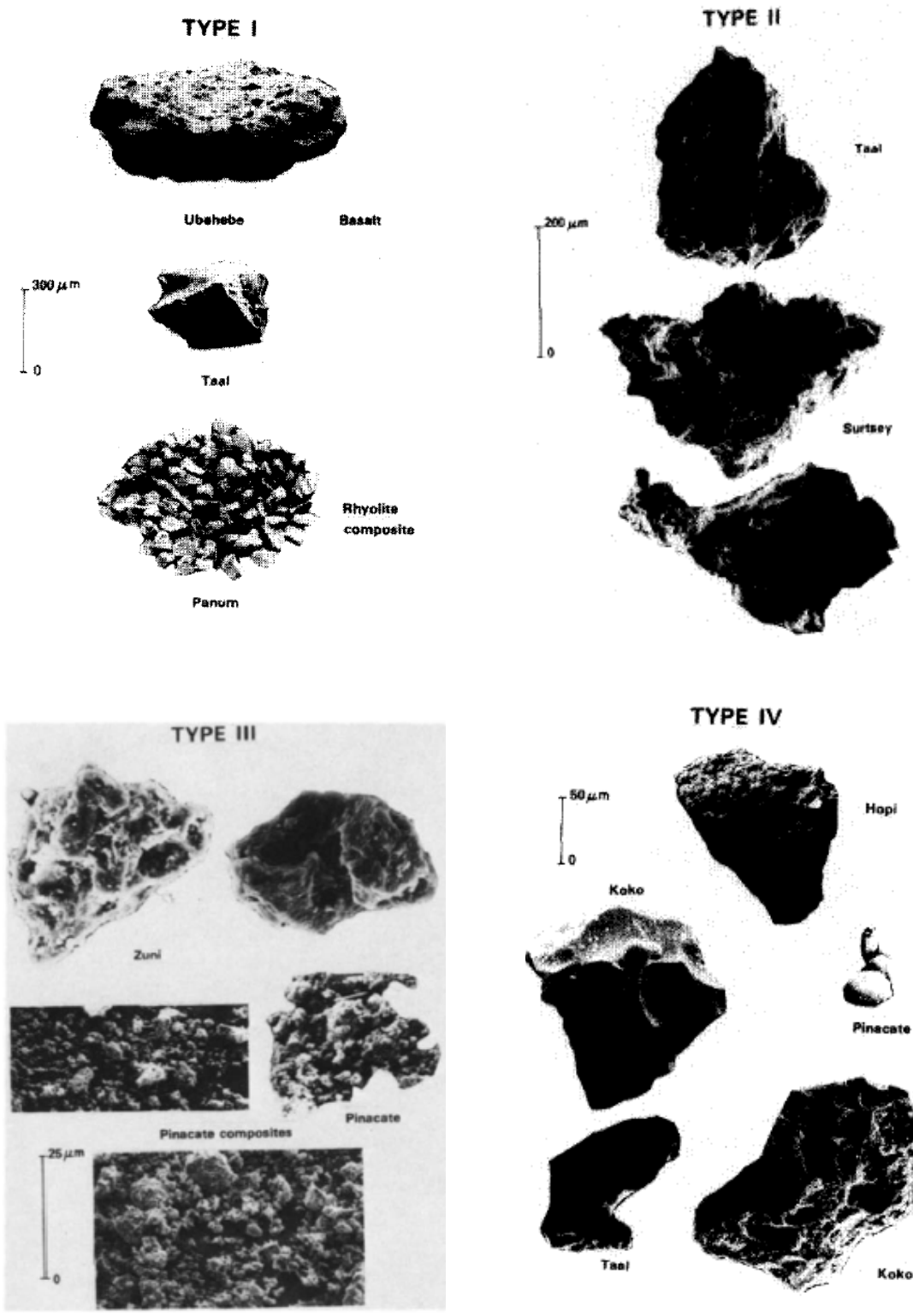

Fig. 10: Tephra shape types according to Wohletz (1983).

Fig. 11: Representation of a large range of Iceland tephra particle shapes (Grimsvötn and Katla volcano) (Maria and Carey, 2002).

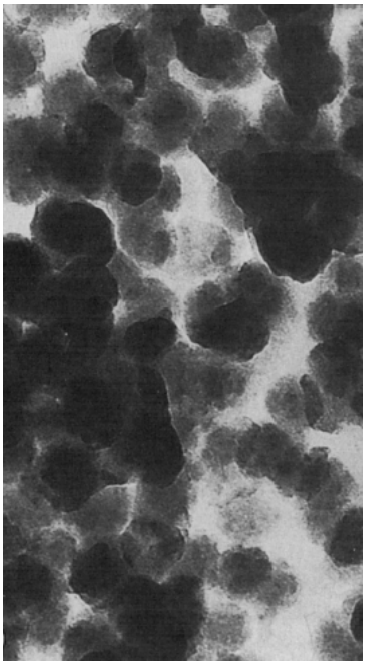

Fig. 12: Amorphous silica structure of a phytolith. The phytolith has roughly spherical silica bodies 35-65 nm (TEM, x 166,000) (Postek, 1981).

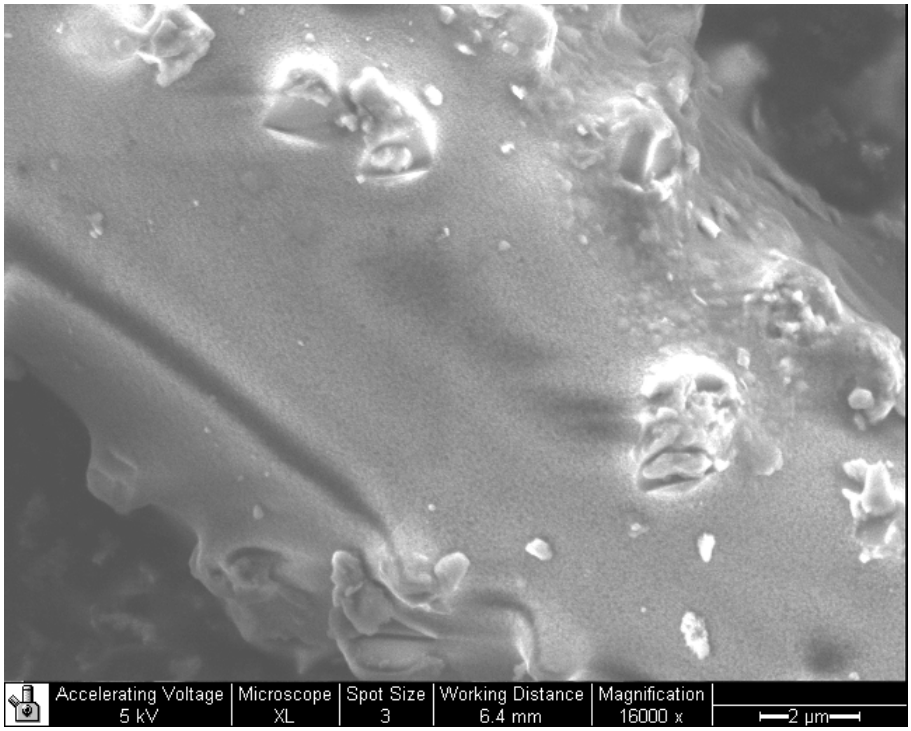

a: Sponge Spicula at 16,000x

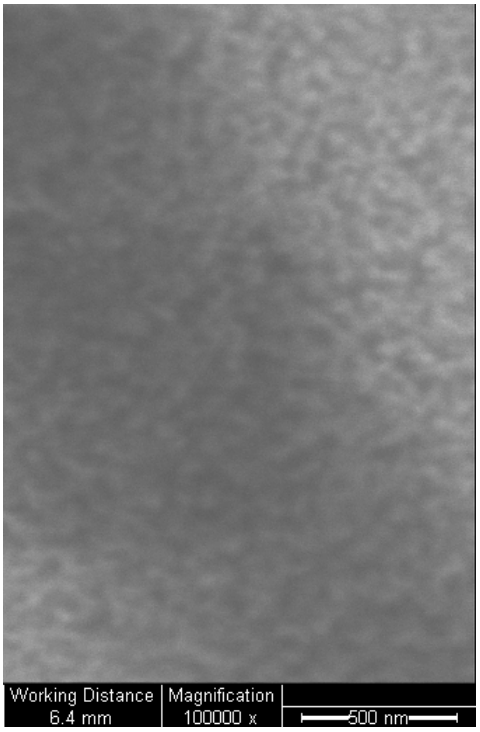

b: Sponge Spicula at 100,000x

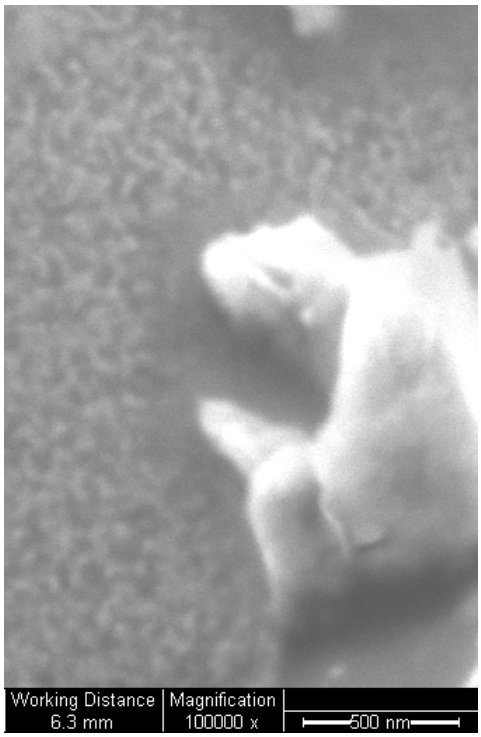

c: Sponge Spicula at 100,000x

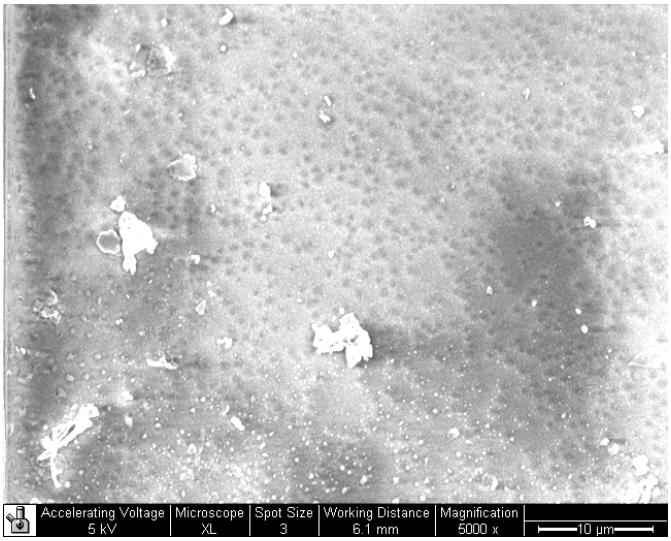

d: Biogenic Silica (sponge spicula) at 5,000x

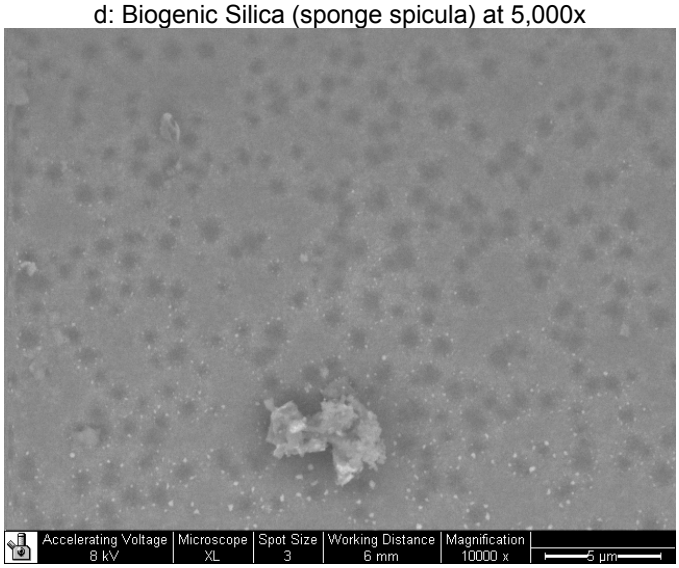

e: Biogenic silica (sponge spicula) at 10,000x

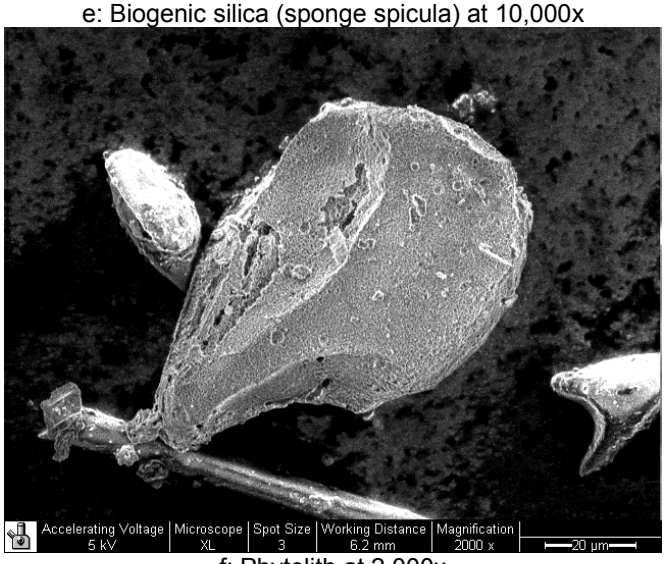

f: Phytolith at 2,000x

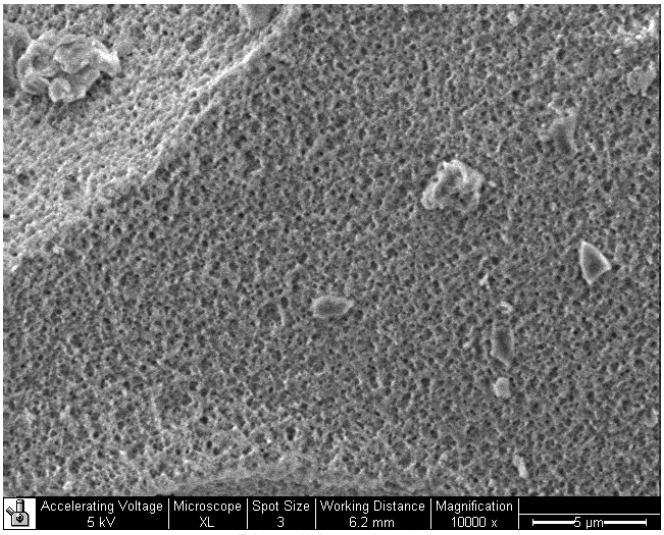

g: Phytolith at 10,000x

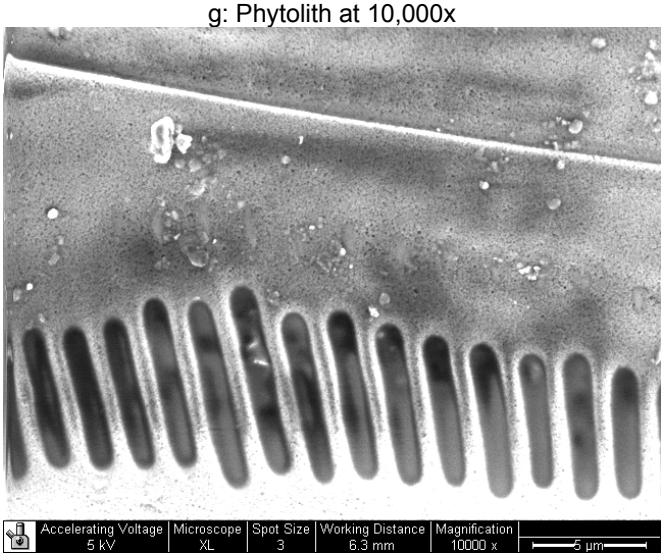

h: Diatom at 10,000x

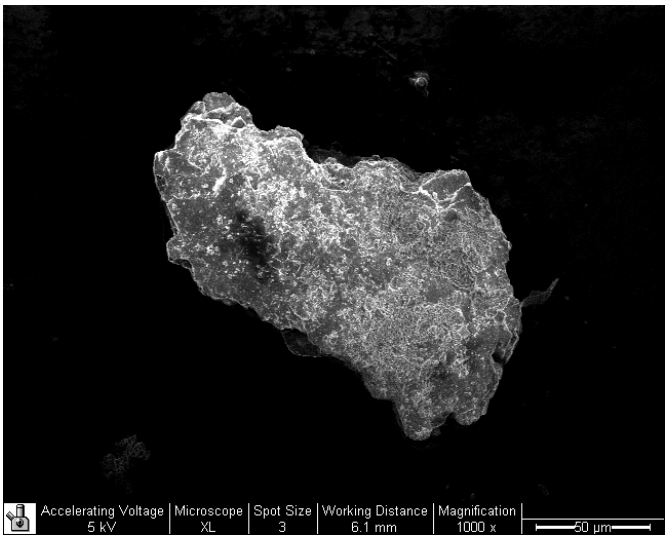

i: Mica particle at 1,000x

j: Mica particle at 75,000x

Fig. 13: Ultra high magnification photomicrographs of Biogenic Silica (a-h) and Mica i,j).

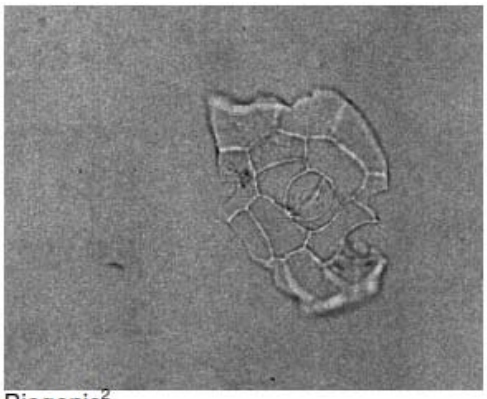

Biogenic[2]

Tephra[1]

Biogenic[2]

Tephra[1]

Tephra[1]

Biogenic[2]

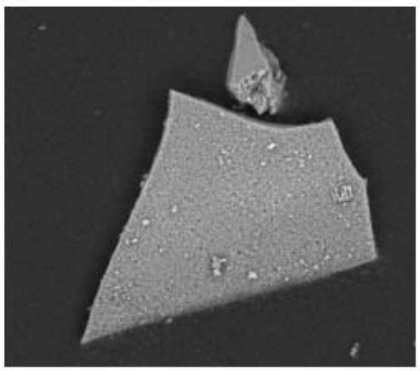

Biogenic[3]

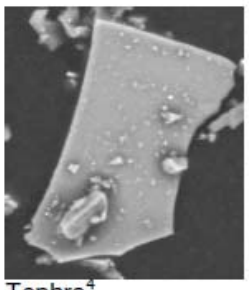

Tephra[4]

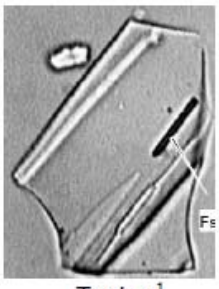

Tephra[1]

Fig. 14: Examples of tephra and biogenic silica with similar morphologies. (van den Bogaard and Schmincke, 2002[1]; The colonial Williamsburg Foundation Phytolith database[2], 2010; own SEMdata[3]; Scherpenhuijsen, 2011[4]).

A problem arises when the optical microscope is used in order to determine the presence of tephra. Tephra and biogenic silica have the same optical properties when looking through the optical microscope and they also have a similar morphology. This results in the fact that biogenic silica cannot always be distinguished from tephra based solely on the morphology when using the optical microscope. This would explain why it was thought that there was tephra present in several depth intervals of the Rheinberg and Zijderveld core. The biogenic silica present was mistaken for tephra. Therefore, chemical analysis of the particles is always needed in order to determine whether the particle is tephra or biogenic silica. An example of a paper where this is not properly done is '*Grain size, areal thickness distribution and controls on sedimentation of the Mount Pinatubo tephra layer in the South China Sea'* (Wiesner et al., 2003). This paper states "... the presence of substantial amounts of amourphous silica, indicating that these (fine size) fractions are dominated by glass shards". It is assumed that these amorphous silica particles are tephra, while there is no chemical analysis of these particles done to support this. They may also be biogenic silica, which, considering the amorphous nature of the particles is also possible.

However, why a peak in the supposed tephra was found remains unknown.

5. Conclusions

- No middle to late Holocene tephra could be found in the Rheinberg and Zijderveld cores. The analysis with the SEM showed that most of the supposed tephra was actually biogenic silica.
- The biogenic silica and tephra have a very similar morphology. Since they have the same optical properties, they cannot always be distinguished from one another based solely on the morphology when using the optical microscope. Therefore, chemical analysis of the particles is always needed in order to determine whether the particle is tephra or biogenic silica.
- There are several possible explanations for the absence of tephra. 1) The ash cloud did not extend as far as these two localities. 2) The deposition occurred by wet fallout. If there was no precipitation at the time the ashcloud passed over the localities, this would explain the absence of tephra. 3) The localities were not suitable for deposition of tephra due to possible presence of running water.

References

Berendsen, H.J.A., Stouthamer, E., 2001. *Paleogeographic development of the Rhine-Meuse delta, the Netherlands. Appendix 3: Channel belts in the Rhine-Meuse delta*. http://www.geo.uu.nl/fg/palaeogeography/downloads

Bergman, J., Wastegard, J., Hammarlund, D., Wohlfarth, B., Roberts, S.J., 2004. *Holocene tephra horizons at Klocka Bog, west central Sweden: aspects of reproducibility in subarctic peat deposits.* Journal of Quaternary Science 19, p. 241-249.

Blockley, S.P.E., Pyne-O'Donnell, S.D.F., Lowe, JJ., Matthews, I.P., Stone, A., Pollard, A.M., Turney, C.S.M., Molyneux, E.G., 2005. *A new and less destructive laboratory procedure for the physical separation of distal glass tephra shards from sediments.* Quaternary Science Reviews 24, p. 1952-1960.

Boygle, J.E., 1994. *Tephra in lake sediments: An unambiguous geochronological marker?* PhD. Thesis, University of Edinburgh, Edinburgh. From: tephrabase.org.

Colonial Williamsburg Foundation Phytolith database, http://research.history.org/Archaeological_Research/Collections/CollArchaeoBot/PhytolithSearch.cfm

Coradin, T., Lopez, P.J., 2003. *Biogenic Silica Patterning: Simple Chemistry of Subtle Biology?* ChemBioChem 4, no. 4, p. 251-259

Davies, S.M., Hoek, W.Z., Bohncke, S.J.P., Lowe, J.J., Pyne O'Donnell, S., Turney, C.S.M., 2005. *Detection of Lateglacial distal tephra layers in the Netherlands.* Boreas 34, p. 123-135.

Dugmore, A.J., Larsen, G., Newton, A.J., 1995. *Seven tephra isochrones in Scotland*. The Holocene 5, p. 257–66. In: Langdon, P.G. and Barber, K.E., 2004. *Snapshots in time: precise correlations of peat-based proxy climate records in Scotland using mid-Holocene tephras.* The Holocene 14, p. 21-33.

Erkens, G., Hoffman, T., Gerlach, R., Klostermann, J., 2001. *Complex fluvial response to late glacial and Holocene allogenic forcing in the Lower Rhine Valley (Germany).* Quaternary Science Reviews 30, p.611-627.

Gouw, M.J.P. and Erkens, G., 2007. *Architecture of the Holocene Rhine-Meuse delta (the Netherlands) – A result of changing external controls.* Geologie en Mijnbouw 86, p. 23-54.

Haflidason, H., Eiriksson, J., van Kreveld, J., 2000. *The tephrochronology of Iceland and the North Atlantic region during the Middle and Late Quaternary: a review.* Journal of Quaternary Science 15, p. 3-22.

Heiken, Grant, 1974. *Atlas of Volcanic ash.* Smithsonian contribution to the earth sciences, no. 12.

Koren, J.H., Svendsen, J.I., Mangerud, J., Furnes, H., 2008. *The Dimna Ash — a 12.8 ^{14}C ka-old volcanic ash in Western Norway*. Quaternary Science Reviews 27, p. 85-94.

Langdon, P.G. and Barber, K.E., 2004. *Snapshots in time: precise correlations of peat-based proxy climate records in Scotland using mid-Holocene tephras.* The Holocene 14, p. 21-33.

Lowe, J.J., 2001. *Abrupt climatic changes in Europe during the last glacial-interglacial transition: the potential for testing hypotheses on the synchroneity of climatic events using tephrochronology.* Global and Planetary change 30, p. 73-84.

Lowe, D.J., Hunt, J.B., 2001. *A summary of terminology used in tephra related studies.* In: Turney, C.S.M., Lowe, J.H., Davies, S.M., Hall, V., Lowe, D.J., Wastegard, S., Hoek, W.Z., Alloway, B. and SCOTAV and INTIMATE MEMBERS, 2004. *Tephrochronology of the Last Termination Sequences in Europe: a protocol for improved analytical precision and robust correlation procedures (a joint SCOTAV-INTIMATE proposal*). Journal of Quaternary Science 19, p. 111-120.

Maria, A., Carey, s., 2002. *Using fractal analysis to quantitatively characterize the shapes of volcanic particles.* Journal of geophysical research 107, no. B11.

Minderhoud, P.S.J., 2008. 5000 years Rhine flooding as recorded in a paleochannel near Rheinberg (Germany) BSc thesis, Faculty of Science, Utrecht University.

Pilcher, J.R., Hall, V.A., McCormac, F.G., 1995. *Dates of Holocene Icelandic volcanic eruptions from tephra layers in Irish peats.* The Holocene 5, p. 103-110.

Pilcher, J.R., Hall, V.A., McCormac, F.G., 1996. *An outline tephra chronology for the Holocene of the north of Ireland*. Journal of Quaternary Science 11, p. 485-494.

Pilcher, J.R. and Hall, V.A., 1996. *A tephra chronology for the Holocene of the north of England.* The Holocene 6, p. 100-105. In: Langdon, P.G., Barber, K.E., 2004. *Snapshots in time: precise correlations of peat-based proxy climate records in Scotland using mid-Holocene tephras.* The Holocene 14, p. 21-33.

Postek, M.T., 1981. *The occurrence of silica in the leaves of Magnolia Grandiflora L.* Botanical Gazette 142, no. 1, p. 124-134.

Scherpenhuijsen, T.T., 2011. *Physical and chemical properties of the Eyjafjallajökull tephra*. BSc thesis, Faculty of Science, Utrecht University.

Van den Bogaard, C., Dörfler, W., Sandgren, P., Schmincke, H.U., 1994. *Correlating the Holocene records: Icelandic tephra found in Schleswig-Holstein (northern Germany).* Naturwissenschaften 81, p. 554-556.

Van den Bogaard, C. and Schmincke, H.U., 2002. *Linking the North Atlantic to central Europe: a high-resolution Holocene tephrochronological record from northern Germany.* Journal of Quaternary Science 17, p. 3-20.

Wastegard, S., Rundgren, M., Schoning, K., Andersson, S., Björck, S., Borgmark, A., Possnert, G., 2008. *Age, geochemistry and distribution of the mid-Holocene Hekla-S/Kebister tephra.* The Holocene 18, p. 539-549.

Wiesner, M.G., Wetzel, A., Catane, S.G., Listanco, E.L., Mirabueno, H.T., 2003. *Grain size, areal thickness distribution and controls*

on sedimentation of the Mount Pinatubo tephra layer in the South China Sea. Bulletin of Volcanology 66, p. 226-242.

Wohletz, K.H., 1983. *Mechanisms of hydrovolcanic pyroclast formation: Grain-size, scanning electron microscopy, and experimental studies.* Journal of volcanology and geothermal research 17, issue 1-4, p. 31-63.

Zillen, L., Wastegard, S., Snowball, I., 2002. *Calendar year ages of three mid-Holocene tephra layers identified in varved lake sediments in west central Sweden.* Quaternary Science Reviews 21, p. 1583-1591.

Appendix A: Chemistry of the analysed particles

Sample	SiO_2	TiO_2	Al_2O_3	Fe_2O_3	MnO	MgO	CaO	Na_2O	K_2O	P2O5
NRB340A	40.75	3.60	17.02	19.27	0.74	10.29	0.43	1.74	5.24	0.94
NRB340B	50.41	0.89	26.80	6.04	1.38	3.29	0.56	1.05	9.01	0.56
NRB340D	60.27	1.09	21.10	1.81	1.31	1.62	0.49	2.14	9.44	0.74
NRB340E	79.90	0.00	12.67	1.28	0.57	1.01	0.25	0.91	2.60	0.81
NRB340F	38.40	2.89	20.16	22.44	0.70	11.06	1.01	1.11	1.91	0.31
NRB340G	79.27	0.94	10.07	1.67	1.05	2.46	0.54	1.19	1.78	1.03
NRB340H	60.42	0.65	20.61	1.79	0.40	1.01	0.61	12.64	0.43	1.45
NRB340J	69.53	0.00	20.07	2.45	0.00	2.15	0.64	1.68	2.38	1.10
NRB340K	13.95	-	5.35	49.71	-	-	-	5.47	-	25.51
NRB340L	48.52	1.18	18.05	14.73	1.24	7.22	0.78	2.60	3.01	2.67
RB340J	76.86	0.70	11.01	4.46	1.20	1.00	0.00	0.79	0.78	3.20
RB340K	61.31	1.16	20.49	6.24	1.80	3.55	1.23	1.95	1.83	0.44
RB350B	53.54	1.69	13.93	17.00	2.39	2.77	1.95	0.99	3.74	2.00
RB350F	53.62	3.29	24.75	5.53	1.19	5.36	0.30	0.87	4.89	0.19
RB360A	40.96	2.09	19.98	19.57	0.66	13.66	1.55	1.17	0.36	0.00
RB360A	38.41	2.43	17.27	24.40	1.09	12.04	2.34	1.10	0.41	0.52
RB360B	52.18	0.27	38.48	3.09	0.97	1.56	1.09	1.14	0.81	0.41
RB360E	47.07	5.76	28.69	10.79	0.72	1.27	0.46	1.19	2.55	1.50
RB360G	54.92	0.51	25.23	8.19	1.10	4.32	1.43	1.60	2.70	0.00
RB360G	50.91	3.74	24.77	8.54	1.13	3.86	0.91	2.00	2.99	1.14
RB360H	57.51	0.78	22.33	6.55	0.74	6.74	1.02	1.09	3.27	0.26
RB360I	54.51	1.38	29.67	6.81	0.39	2.80	1.61	0.95	1.23	0.63
RB360J	49.19	0.82	30.26	5.33	0.00	11.86	1.67	0.40	0.47	0.00
RB360K	82.24	0.61	9.85	0.91	0.30	1.02	0.87	1.25	2.45	0.51
RB360L	55.93	1.07	15.60	6.50	0.46	12.52	1.94	3.40	2.33	0.24
RB547A	51.13	1.02	11.84	25.77	0.93	3.97	1.91	1.67	0.58	1.20
RB547B	52.86	1.13	19.06	16.77	0.86	1.66	1.24	1.74	3.53	1.14
RB547C	52.63	0.86	13.38	25.91	0.70	2.41	1.40	0.20	1.54	0.97
RB547C	52.84	1.79	18.91	16.32	1.94	2.13	1.59	2.14	1.94	1.49
RB547E	52.47	1.79	17.36	16.03	0.43	1.78	5.12	0.72	2.90	1.40
RB547E	54.12	1.00	25.47	7.31	1.22	3.53	1.31	2.30	2.25	1.49
RB547F	61.06	0.00	20.28	7.73	0.00	6.20	0.25	1.54	2.38	0.57
RB547F	56.50	0.40	20.41	15.12	0.00	4.39	0.64	0.81	1.72	0.00
RB547BA	70.71	0.92	8.54	9.98	0.61	2.17	1.40	2.62	1.33	1.72
RB547BB	50.44	0.93	33.13	2.91	0.00	2.55	0.47	1.38	7.75	0.45
RB547BC	51.59	0.00	36.69	2.17	0.00	2.97	0.67	0.60	5.31	0.00
RB547BD	53.17	0.52	7.84	27.60	1.99	0.96	1.80	3.49	1.23	1.39
RB547BE	69.27	0.00	23.19	0.91	0.00	1.23	1.08	2.13	0.72	1.48
RB547BF	59.44	1.95	23.45	10.45	0.00	0.95	1.15	0.00	2.18	0.44
RB547BG	74.65	0.75	14.69	3.38	0.45	2.18	0.68	1.23	1.49	0.49
ZV095B	69.61	0.72	10.08	9.50	1.29	1.08	0.63	2.24	0.58	-
ZV095C	20.18	5.45	9,82	39.79	0.99	0.96	0.66	0.73	1.01	20.42
ZV095D	48.34	1.15	18.94	15.35	1.45	0.66	0.60	1.09	6.55	5.87
ZV095E	60.18	0.40	20.71	1.64	0.45	1.37	0.30	1.62	12.12	1.22

Sample	SiO_2	TiO_2	Al_2O_3	Fe_2O_3	MnO	MgO	CaO	Na_2O	K_2O	P2O5
ZV095F	61.22	1.04	18.84	2.66	1.03	0.69	0.41	0.78	11.95	1.38
NZV95E	15.08	1.28	7.66	45.72	0.99	1.29	1.11	3.06	1.20	22.63
NZV95F	28.79	1.81	17.43	23.28	0.30	2.54	1.17	5.25	2.21	17.22
NZV95I	62.61	2.25	9.97	9.02	2.40	3.36	0.68	7.23	0.87	1.61
NZV95J	86.03	0.00	4.18	1.42	0.00	0.75	1.57	2.10	1.18	2.77
NZV95L	16.49	2.02	10.96	33.73	1.72	2.62	1.61	6.52	1.23	23.11
ZV195A	92.34	0.79	3.00	1.05	0.83	0.69	0.44	0.56	0.31	-
ZV195B	94.39	0.00	1.66	0.34	1.26	0.89	0.00	1.31	1.16	-
ZV195G	62.69	0.76	19.75	0.76	0.84	1.09	0.32	1.49	11.95	0.35
ZV195I	45.68	0.88	38.53	1.45	0.25	1.61	0.22	1.43	9.49	0.46
ZV280A	86.53	0.00	8.46	0.00	0.00	1.72	0.00	2.51	0.79	0.00
ZV280B	61.51	0.54	23.34	3.34	0.00	5.30	0.68	3.31	0.33	1.65
ZV280C	48.11	1.19	17.21	14.94	0.00	11.25	0.97	3.94	1.67	0.73
ZV280D	61.90	0.94	9.92	15.58	1.40	3.29	0.68	3.99	0.79	1.51
ZV280E	63.93	0.00	23.94	2.79	0.00	5.68	0.73	2.46	0.21	0.72
ZV280F	93.81	0.00	2.59	0.00	0.00	1.49	0.34	1.10	0.00	0.67
ZV280BA	95.56	0.49	0.00	0.00	0.00	0.00	0.72	0.00	0.23	0.00
ZV280BC	88.14	1.39	2.32	2.24	1.11	0.68	0.91	1.18	0.49	1.53
ZV280BD	97.17	0.52	1.28	0.00	0.00	0.00	0.44	0.24	0.35	0.00
ZV280BE	85.32	0.27	3.78	1.69	1.35	1.21	1.00	3.49	0.67	1.21
ZV280BF	50.92	0.00	35.60	5.43	0.00	3.75	0.58	1.87	1.31	0.53
ZV280BG	92.37	0.68	2.03	0.00	0.00	0.62	0.48	2.47	0.51	0.83
ZV280BH	92.82	0.00	2.25	0.00	1.00	0.40	0.00	3.53	0.00	0.00
ZV280BI	95.55	0.26	1.50	0.00	0.00	0.17	0.15	0.94	0.40	1.02
ZV280BJ	96.93	0.53	1.34	0.00	0.00	0.50	0.27	0.18	0.25	0.00
ZV280BK	96.43	0.38	1.61	0.00	0.00	0.39	0.45	0.28	0.47	0.00
As6*	61.93	1.65	16.11	7.11	-	2.31	3.30	5.58	2.01	-

N = particles picked underneath the binocular.

* Scherpenhuijsen, 2011. Tephra particle of the Eyjafjallajökull.